Science World Journal Vol. 21(No 2) 2026 https://dx.doi.org/10.4314/swj.v21i2.47
www.scienceworldjournal.org
ISSN: 1597-6343 (Online), ISSN: 2756-391X (Print)
Published by Faculty of Science, Kaduna State University

Full Length Research Article

ASSESSMENT OF UNCERTAINTIES IN THE COMPUTATION OF ATMOSPHERIC CORRECTION PARAMETERS FOR LANDSAT 5 TM AND LANDSAT 7 ETM+ THERMAL BAND

Barnabas O. Morakinyo

Department of Surveying & Geoinformatics, Faculty of Environmental Sciences, BAZE University, Abuja, Nigeria

*Corresponding Author Email Address: barnabas.ojo@bazeuniversity.edu.ng

ABSTRACT
This research examines the uncertainties present when computing atmospheric correction parameters (upwelling ($L_i\uparrow$) and downwelling ($L_i\downarrow$) radiances, and transmittance (τ)) for the 9 flaring sites in Rivers State, Nigeria, and to estimate the total uncertainty introduced into the land surface temperature (LST) when they are applied. Eight (8) Landsat 5 Thematic Mapper (TM) and Twenty-Four (24) Landsat 7 Enhanced Thematic Mapper Plus (ETM+) from 18 August 2000 to 08 March 2013, with less than 3 percent (%) cloud contamination, were considered to evaluate a trend. Option B of the Atmospheric Correction Parameter (ATMCORR) Calculator was adopted to obtain $L_i\uparrow$, $L_i\downarrow$, and τ for the thermal band (band 6) of the Landsat scenes analysed. The $L_i\uparrow$, $L_i\downarrow$, and τ obtained were applied to the calibrated at-sensor radiance band 6 (high gain) data to compute the surface-leaving radiance $L_i(T_i)$ with the emissivity (ε) of each station estimated by using standard values for determined land surface cover. The Planck equation was inverted using the Landsat calibration constants to derive the LST. To determine the uncertainties introduced into the retrieved LST, the difference between the computed mean surface temperature (ST) measured at each flaring site during ground truthing and the combined average LST retrieved from the Landsat datasets is applied. The results show that the larger the % of water body at the site, the higher the uncertainty in LST, and vice versa. Bonny LNG has the highest error of 24.712 K, Eleme II has the lowest value of 0.752 K. Based on the results obtained, it can be concluded that the ATMCORR Calculator can provide an automated method to derive $L_i\uparrow$, $L_i\downarrow$, and τ for Landsat 5 and Landsat 7 thermal band for generating LST in the Niger Delta, Nigeria.

Keywords: Multispectral and Thermal Remote Sensing, Atmospheric Correction, Atmospheric Correction Parameters (ATMCORR) Calculator, Emissivity, Land Surface Temperature (LST), Niger Delta.

INTRODUCTION

Atmospheric correction (AC) plays a critical role in the pre-processing of remote sensing data (Zhu & Xia, 2023). The ground spectral information derived from satellite images is distorted by atmospheric effects (Emberton et al., 2015); hence, AC is necessary to reduce interference (Kondratyev et al., 1992; Chavez, 1996; Emberton et al., 2015). Also, AC is necessary for most applications involving remote sensing inversion (Campbell et al., 2011; McCarthy et al., 2012; Zhu et al., 2013; Liu et al., 2016). Accurate conversion from top-of-atmosphere (TOA) reflectance to surface reflectance (SR) is a critical pre-processing step for quantitative remote sensing applications, and this process is called atmospheric correction (Hu et al., 2014).

Changes in atmospheric conditions or in sun and sensor elevations (and hence the path through the atmosphere) will alter the amount of light scattered and absorbed by the atmosphere (Liu et al., 2016). These changes affect both the amount of light illuminating the surface and the amount of light reaching the sensor (Schott, 1989; Flood et al., 2013). Atmospheric effects on the signal include a range of scattering and absorption processes and depend on the angles between the sun, surface, and satellite (Morakinyo, 2015). These effects are assumed to be well modelled by widely available atmospheric radiative transfer models (Flood et al., 2013).

Most atmospheric gases and aerosols cause scattering, absorption, and polarization of solar radiation, leading to changes in the incoming irradiance (Liou, 2002; Kokhanovsky & de Leeuw, 2009). Indeed, through its path from the TOA to the Bottom of Atmosphere (BOA) (downwelling path), and back to the sensor once reflected (upwelling path), the energy is scattered and absorbed, causing the extinction of the initial energy flux (exoatmospheric spectral irradiance (ESUN) ($Wm^{-2}\mu m^{-1}$)) (Schott, 1989; Padro et al., 2017). This phenomenon of light extinction is quantified with the spectral magnitude known as atmospheric transmittance (τ_λ) (dimensionless) (Padro et al., 2017). Transmittance depends on the spectral atmospheric Total Optical Depth (TOD) ($\tau_{o\lambda}$), as greater TOD implies lower transmittance (Schott, 1989). Transmittance is also dependent on the zenith angle of the illumination vector (the greater the angle, the smaller the transmittance) (Padro et al., 2017).

Simultaneously, scattering leads to energy re-distribution, and a part of this energy flux contributes as diffuse radiance (atmospheric spectral radiance, Latmλ ($Wm^{-2}sr^{-2}m^{-1}$)) to the radiance received both at the Earth's surface and at the sensor (Schneider & Mauser, 1996). Therefore, in general terms, atmospheric corrections of the signal reflected from the Earth's surface have two main unknowns (wavelength dependent) (Turner et al., 1971; Schneider & Mauser, 1996): the TOD that weakens the signal, and the atmospheric radiance that contributes to the signal in addition to the reflected beam (Padro et al., 2017).

The satellite measured thermal radiance L_λ consists of the following components (Schott, 1989):
$L_\lambda = (\varepsilon_\lambda L_{w\lambda} + r_\lambda L\downarrow_\lambda)T_\lambda + L\uparrow_\lambda$
ε_λ = Emissivity of water; $L_{w\lambda}$ = Long radiation from the water surface; r_λ = Reflectivity of water $(1-\varepsilon_\lambda)$; $L\downarrow_\lambda$ = Downward longwave atmospheric radiation; T_λ = Transmissivity of the atmosphere; $L\uparrow_\lambda$ = Upward longwave atmospheric radiation.

Longwave radiation emitted by the water body is reduced by atmospheric transmittance and water emissivity (Markham & Baker, 1985; Schott, 1989; Schneider & Mauser, 1996). The atmosphere not only absorbs the thermal radiation ($L\uparrow_\lambda$), but it also emits it according to its own temperature and emissivity (Schott, 1989; Schneider & Mauser, 1996). In addition, the longwave atmospheric radiation reflected ($r_\lambda L\downarrow_\lambda)T_\lambda$) at the water surface constitutes the third component of the sensor measured signal (Schott, 1989; Schneider & Mauser, 1996).

Furthermore, an AC is required to retrieve the real surface parameters by removing the atmospheric effects, such as (potentially) thin clouds (Inamdar et al., 2008); molecular and aerosol scattering, absorption by gases (such as water vapour, ozone, oxygen) and aerosol, and sometime also the correction for cloud shadows, upward emission of the radiation from the Earth surface (Qin et al., 2011); environmental radiance which produces the adjacency effects, variation of illumination geometry including the Sun's azimuth and zenith angles, and ground slope (Mather, 2004). Removing the effects of the atmosphere in the thermal region is an essential step when using thermal band imagery for absolute temperature studies, i.e., to correct the TOA radiance or temperature to the surface-leaving radiance (L_λ) or temperature (Barsi et al., 2003; Otukei & Blaschke, 2011; Qin et al., 2011). The emitted signal from the ground can be both attenuated and enhanced by the atmosphere (Barsi et al., 2005**)**.

TOA measurements must be corrected from atmospheric and emissivity effects to convert brightness temperatures into LSTs (Galve et al., 2018). Various atmospheric correction methods have been proposed for Thermal Infrared (TIR) bands, depending on sensor characteristics (Galve et al., 2018). Split-window methods apply to those sensors with at least two spectral channels, usually at 11 and 12 $\times \mu$m (Becker & Li, 1995). This has been the correction method traditionally applied to the National Oceanic and Atmospheric Administration (NOAA)/Advanced Very High Resolution Radiometer (AVHRR) (Price, 1984; Becker & Li, 1990; Becker & Li, 1995; Coll & Caselles, 1997), Earth Observation Satellite (EOS) Terra-Aqua/Moderate Resolution Image Spectroradiometer (MODIS) (Wan, 1999; Wan, 2008; Galve et al., 2008), Environmental satellite (Envisat)/Advanced Along Track Scanning Radiometer (AATSR) (Prata, 2002; Galve et al., 2008) or the Meteosat Second Generation (MSG)/Spinning Enhanced Visible and Infrared Imager (SEVIRI), (Madeira, 2002; Trigo et al., 2008; Niclòs et al., 2011) or Suomi National Polar-Orbiting Partnership (s-NPP)/Visible Infrared Imaging Radiometer Suite (VIIRS) (Yu et al., 2005; Niclòs et al., 2018).

The novelty of this study is that no publication has been made on the application of the Atmospheric Correction Parameters (ATMCORR) tool for the computation of atmospheric correction parameters for Landsat 5 Thematic Mapper (TM) and Landsat 7 Enhanced Thematic Mapper Plus (ETM+) thermal band datasets for the Niger Delta, Nigeria. Also, the methodology adopted in this research has not been used in any prior publication. Furthermore, the results obtained will serve as a reference for other researchers in the related fields in Nigeria and in the world at large, i.e., this paper has added to the literature on Landsat 5 and Landsat 7 sensors; single thermal band atmospheric correction; and the computation of the atmospheric correction parameters for Landsat 5 and Landsat 7 single thermal band (band 6) by the ATMCORR tool.

Furthermore, when the sensor is provided with three or more bands in the TIR domain, the Temperature and Emissivity Separation (TES) method (Gillespie et al., 1998) can be applied. Once corrected from atmospheric effects, at-ground TIR radiances are used as input in the TES approach (Coll et al., 2007). The TES method was originally developed for the EOS-Terra/Advanced Spaceborne Thermal Emission and Reflection Radiometer (ASTER) (Gillespie et al., 1998; Coll et al., 2007). LST products of MODIS (MOD21) and s-NPP/VIIRS are also based on the TES technique (Hulley et al., 2014; Coll et al., 2016).

Sensors with a single channel in the TIR domain require atmospheric-effect simulations based on estimates of atmospheric water vapour and air temperature profiles (Galve et al., 2018), so single-channel (SC) techniques are required (Galve et al., 2018). Various sources can be used to obtain the required atmospheric profiles (Galve et al., 2018). Launching a local atmospheric sounding close in time to the sensor overpass is the most accurate approach, although it is rarely possible (Galve et al., 2018). Currently, atmospheric profiles can be obtained from satellite sounders such as the EOS-Aqua/Air Infrared Sounder (AIRS). MODIS product MOD07 is also available (Galve et al., 2018). However, the sensor of interest is not always coincident with the sounder overpass, and the results are undesirable (Coll et al., 2012).

Some meteorological models forecast atmospheric profiles with a fixed periodicity and very low spatial resolution (3-6 h and 0.25°-2° latitude/longitude) (Niclòs, et al., 2018). Li et al. (2013**)** compared the results obtained between the National Center for Environmental Prediction (NCEP) and MOD07 for Huan-Jing 1B /Infrared Scanner (HJ-1B/IRS) data in two sites in China, covering water, bare soil, wheat, and corn, and their results yielded differences around $\pm$1.2 K for both sources. Also, Meng & Cheng (2018) evaluated several reanalysis products from the National Center for Environmental Prediction (NCEP) using 32 Landsat 8 Thermal Infrared Sensor (L8-TIRS) images over Gansu Province, China. Almost no difference in terms of LST is observed by these authors with RMSE values within $\pm$2 K. Similar results were obtained by Duan et al. (2018), over sands, grasslands, and snow, using NCEP data in conjunction with the Moderate-Resolution Atmospheric Radiance and Transmittance (MODTRAN) 5 code to correct L8-TIRS data from atmospheric effects.

Various methods have been developed to solve the AC process for TIR data dedicated to single-channel sensors. The available methods can be classified into four categories: (1) The single-channel algorithm, which requires total atmospheric water content values only (Jiménez-Muñoz et al., 2003); (2) The mono-window algorithm, which requires air temperature data only (Qin et al., 2001); (3) The look-up tables (LUT) approach, which supposes an exhaustive learning database (Jiménez-Muñoz et al., 2009); and (4) The physical approach, which requires the calculation of atmospheric parameters with a radiative transfer model and demands detailed knowledge of the atmospheric profile (Barsi et al., 2003; Coll et al., 2010).

As the Landsat 5 Thematic Mapper (TM) and Landsat 7 Enhanced Thematic Mapper Plus (ETM+) instruments only have a single

Science World Journal Vol. 21(No 2) 2026 https://dx.doi.org/10.4314/swj.v21i2.47
www.scienceworldjournal.org
ISSN: 1597-6343 (Online), ISSN: 2756-391X (Print)
Published by Faculty of Science, Kaduna State University

thermal band (band 6 with 10.40-12.50 μm wavelength), there is no inherent methodology to correct for atmospheric effects, unlike with multiband thermal sensors that utilise the differential absorption in adjacent bands (Wan & Dozier, 1996; Qin et al., 2001). Therefore, ancillary atmospheric data are required. The use of atmospheric radiative transfer models to remove atmospheric effects from Landsat imagery has been demonstrated in an operational context by several other authors, including Masek et al. (2006), Schroeder et al. (2006), and Vicente-Serrano et al. (2008).

The gaps before this research are that, in the Niger Delta, limited research on the removal of atmospheric effects from the thermal bands of Landsat 5 TM and Landsat 7 ETM+ data has been published to date. No studies applied the Atmospheric Correction Parameters (ATMCORR) Calculator tool methodology for the derivation of AC parameters (upwelling ($L_i\uparrow$), downwelling ($L_i\downarrow$) radiances and transmittance (τ)) for Landsat 5 and Landsat 7. Therefore, the two basic research questions for this study are: (1) How accurately can the ATMCORR Calculator derive the upwelling ($L_i\uparrow$), downwelling ($L_i\downarrow$), and transmittance (τ) for Landsat 5 and Landsat 7 thermal band data in the Niger Delta, Nigeria? (2) What is the maximum error introduced into the Land Surface Temperature (LST) generated from using the derived $L_i\uparrow$, $L_i\downarrow$, and τ obtained from the ATMCORR Calculator? Based on these questions, the primary aim of this study was to evaluate the total uncertainties introduced into the LST(s) when the derived $L_i\uparrow$, $L_i\downarrow$, and τ are applied for the 9 flaring sites in Rivers State of the Niger Delta region (Nigeria). The specific objectives set to answer the research questions are: (1) Derivation of $L_i\uparrow$, $L_i\downarrow$, and τ from the ATMCORR Calculator; (2) Retrieval of the LST from Landsat 5 and Landsat 7 using the derived $L_i\uparrow$, $L_i\downarrow$ and τ from the ATMCORR Calculator; (3) Validation of the retrieved LST using the insitu surface temperature (ST) measured data; (4) Determination of the amount of uncertainties introduced into the LST by applying the calculated $L_i\uparrow$, $L_i\downarrow$ and τ .

MATERIALS AND METHODS

Case Study Sites

This study focuses on nine (9) oil and gas facilities located in Rivers State, Nigeria. The selection of these flare sites was based on the facility's function, such as refineries, liquefied natural gas (LNG) plants, flow stations, oil and gas terminals, and oil wells. Those chosen include: Eleme Refinery I and II Petroleum Companies; Bonny LNG plant; Onne, Rukpokwu, Umurolu, Obigbo, and Chokocho Flow Stations; and Elem Kalabari oil well (Figure 1). Figure 2 A-E shows a typical flaring of gas at Eleme Petroleum Company Refinery 1, Bonny LNG Plant, Obigbo Flow Station, Rukpokwu Flow Station, and Chokocho Flow Station, respectively (Google Earth, 2026). Each site was investigated as a 12-by-12 km area. Table 1 shows the coordinates of the location of each of the flare stacks within each facility.

Table 1: Coordinates of the Flare Stack Within Each Facility

S/N	Name of the facility	Flare stack coordinates		Flare stack height (m)	Facility size	% of water body at the Site
		Latitude (Ø)	Longitude (λ)			
1.	Eleme Refinery I	4.729	7.119	50	1.6 × 1.1 km	25
2.	Eleme Refinery II	4.762	7.111	65	2.2 × 1.3 km	15
3.	Onne Flow Station	4.712	7.141	3.5	175 × 130 m	48
4.	Bonny (LNG) Plant	4.414	7.140	25	4.2 × 2.8 km	90
5.	Rukpokwu Flow Station	4.930	7.016	25	350 × 350 m	34
6.	Umurolu Flow Station	4.829	7.109	60	4.2 × 2.4 km	50
7.	Obigbo Flow Station	4.892	7.120	22	650 × 650 m	48
8.	Elem Kalabari oil well	4.554	6.978	22	350 × 250 m	89
9.	Chokocho Flow Station (Centre station)	5.008	7.019	21	350 × 120 m	69

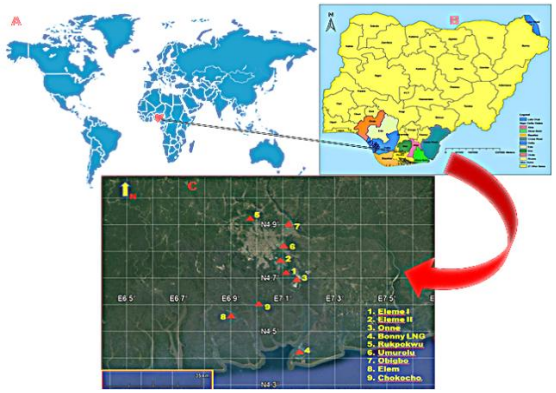

Figure 1: A) Map of Nigeria in Africa (Morakinyo & Akubue, 2026); B) Map of Rivers State in the Niger Delta Region, Nigeria (Google Earth, 2026); C) Locations of the Case Study Sites (Google Earth, 2026)

Science World Journal Vol. 21(No 2) 2026 https://dx.doi.org/10.4314/swj.v21i2.47
www.scienceworldjournal.org
ISSN: 1597-6343 (Online), ISSN: 2756-391X (Print)
Published by Faculty of Science, Kaduna State University

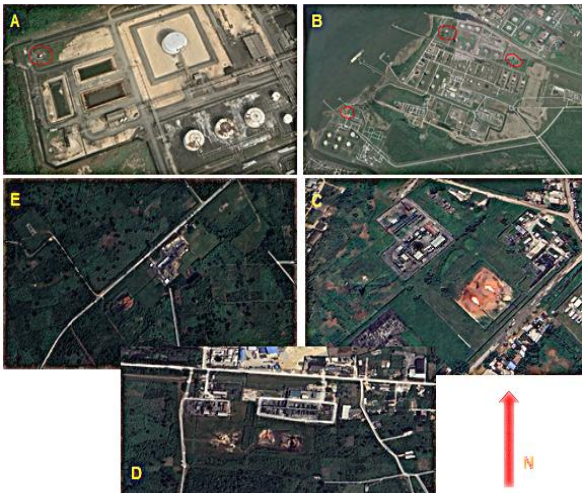

Figure 2: Typical Gas Flaring at A) Eleme Petroleum Company Refinery 1; B) Bonny LNG Plant; C) Obigbo Flow Station; D) Rukpokwu Flow Station, and E) Chokocho Flow Station (Google Earth, 2026)

Data Used

The U.S. Geological Survey (USGS) data archive was systematically searched for scenes with < 3 percent (%) cloud contamination. All the sites are located within a single Landsat scene (Path 188, Row 057), with the results of the search being eleven (11) Landsat 5 TM and Twenty-Six (26) Landsat 7 ETM+ scenes from 04 October 1984 to 08 March 2013. The imagery was downloaded from the USGS Earth Resources Observation and Science (EROS) Data Centre website (http://earthexplorer.usgs.gov/) using the Glovis/Earth Explorer interfaces. The processing level for all the scenes is L1T, which means systematic radiometric correction, and geometric correction using both ground control points (GCPs) and a digital elevation model was applied (USGS, 2015; Morakinyo, 2025a, b; Morakinyo, 2026).

METHODS

Atmospheric Correction Parameter (ATMCORR) Calculator

In order to obtain the AC parameters ($L_i\uparrow$, $L_i\downarrow$ and τ_i) at a given geographical point for band 6 of Landsat 5 TM and Landsat 7 ETM+, the ATMCORR Calculator developed by Barsi et al. (2003) and Barsi et al. (2005), which uses National Center for Environmental Prediction (NCEP) data, and made available to the public at http://atmcorr.gsfc.nasa.gov (Coll et al., 2010), was employed. However, according to Barsi et al. (2005), the limitations of the ATMCORR Calculator are as follows: (1) The ATMCORR Calculator generates parameters for a single point. This may be sufficient to describe the atmosphere across a whole Landsat scene in some cases, but where there is a considerable elevation change, more than one run of the Calculator may become necessary. (2) There is no automatic check for clouds or discontinuities in the interpolated atmosphere. Therefore, the profiles contained in the emailed summary file need to be checked for the problems; (3) The NCEP data in the format currently used is not available for the entire Landsat 5 and Landsat 7. The NCEP holdings include all dates since 01 March 2000; (4) The interpolation in time and space is linear, which may not be the most appropriate method for sampling weather fronts or areas with significant diurnal heating cycle; and (5) The emissivity (ε) of the target must be known in order to calculate LST.

The initial validation of the ATMCORR Calculator by Barsi et al. (2005) showed a systematic error of $>$ 1.5 K, and a bias of 0.5 $\pm$ 8 K for LSTs generated after correction. Coll et al. (2010) demonstrated high accuracy of the ATMCORR Calculator using Landsat 7 data over fully covered rice fields. They compared the modelled values with ground-based LST measurements, showing differences of ±1K.

Operational Principle of ATMCORR Calculator

The ATMCORR Calculator is a single-channel method that applies the MODTRAN algorithm (Berk et al., 2011) to enable users to accurately retrieve LST from Landsat 5 and Landsat 7 thermal data (Barsi et al., 2003; Barsi et al., 2005; Barsi, 2014). It uses NCEP to provide atmospheric data for 28 altitudes; NCEP has global coverage, but a coarse 1° by 1° grid (spatial resolution) and 6 hour time step (temporal resolution). Currently, the ATMCORR Calculator only provides AC parameters for dates from 01 March 2000, as this is when the dataset began (McCarville et al., 2011; Morakinyo, 2015; Morakinyo, 2026).

The Calculator requires a specific date, time, and location as the input (Figure 3) (Table 2), and has 2 methods for resampling the grid to the specific site: (1) Use the atmospheric profile for closest integer Lat./Long (Figure 4A); and (2) Use interpolated atmospheric profile for given Lat./Long (Figure 4B). The first method extracts the grid corner closest to the input location for the 2 temporal samples bounding the input time and interpolates to the given time. The second option extracts profiles for the 4 grid corners surrounding the location, before and after the specified time. The corner profiles are interpolated at each time, and the resulting time profiles are then interpolated to produce a single profile (Barsi et al., 2003). The figure shows the AC Parameter Calculator Web Interface (Barsi et al., 2003).

Furthermore, the user-supplied local surface conditions will be used, and the lower layers of the atmosphere will be interpolated from 3 km above sea level down to the surface to remove any discontinuities (Barsi et al., 2003). Another option is to choose between a summer and a winter standard atmosphere for the upper layer (Barsi et al., 2005). In addition, the user can select the TM bandpass, the ETM+ bandpass, or no spectral bandpass; in the latter case, only the interpolated atmospheric profiles for use in a radiative transfer model are output (Barsi et al., 2003; Barsi et al., 2005; Barsi, 2014). The resulting integrated $L_i\uparrow$, $L_i\downarrow$, and τ, along with all the atmospheric data used to generate the results, are output to the browser and emailed to the user.

For this research, the coordinate of each flare station (latitude (Ø) and longitude (λ)), date of satellite observation (year, month, date), and time of data acquisition (hours and minutes) was inputted into the calculator. Option B, which is to use an interpolated atmospheric profile for the given (Ø) and (λ), was chosen alongside the mid-latitude summer standard atmosphere. Landsat 5 band 6 and Landsat 7 band 6 spectral response curves were chosen for Landsat 5 and Landsat 7 data, respectively. In less than 4 minutes, the supplied data was processed, and the result was displayed on the computer screen and sent to the supplied e-mail address

Science World Journal Vol. 21(No 2) 2026 https://dx.doi.org/10.4314/swj.v21i2.47
www.scienceworldjournal.org
ISSN: 1597-6343 (Online), ISSN: 2756-391X (Print)
Published by Faculty of Science, Kaduna State University

(Figure 5B). Figure 5A shows the locations of the 9 investigated flare sites in (Ø) and (λ).

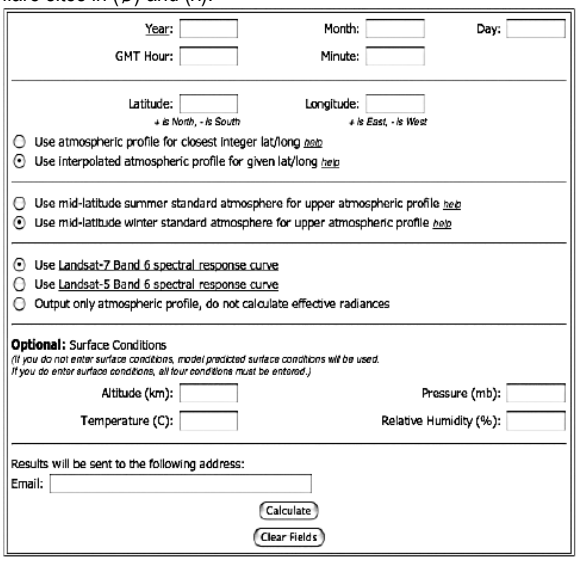

Figure 3: The Atmospheric Correction Parameter Calculator Web Interface (Barsi et al, 2003)

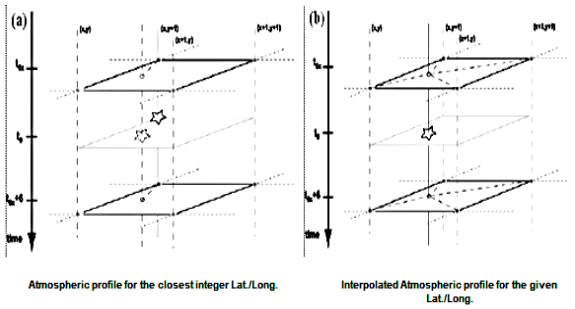

Figure 4: A) Atmospheric Profile for the Closet Integer Lat./Long.; B) Interpolated Atmospheric Profile for the Given Lat./Long (Barsi et al, 2003)

Table 2: Date and Time of Some Landsat 7 ETM+ Scenes used for Processing $L\uparrow$, $L\downarrow$ and τ

Scene Identity No.	Acquired Date	Acquired Time (h:m)	Path/ row	Processing Level
LE7188057200 0064SGS00	March 4, 2000	09:37	188/ 057	L1T
LE7188057200 0336AGS00	December 1, 2000	09:35	188/ 057	L1T
LE7188057200 2037SGS00	February 6, 2002	09:34	188/ 057	L1T
LE7188057200 2325SGS00	November 21, 2002	09:33	188/ 057	L1T
LE7188057200 4043ASN01	February 12, 2004	09:34	188/ 057	L1T
LE7188057200 4331ASN00	November 26, 2004	09:34	188/ 057	L1T
LE7188057200 6016ASN00	January 16, 2006	09:35	188/ 057	L1T
LE7188057200 6352ASN00	December 18, 2006		188/ 057	
LE7188057200 8006ASN00	January 6, 2008	09:35	188/ 057	L1T
LE7188057200 8326ASN00	November 21, 2008	09:34	188/ 057	L1T
LE7188057201 0043ASN00	February 12, 2010	09:37	188/ 057	L1T
LE7188057201 0347ASN00	December 13, 2010	09:38	188/ 057	L1T
LE7188057201 2017ASN01	January 17, 2012	09:39	188/ 057	L1T
LE7188057201 2225ASN00	August 12, 2012	09:40	188/ 057	L1T
LE7188057201 3003ASN00	January 3, 2013	09:41	188/ 057	L1T
LE7188057201 3067ASN00	March 8, 2013	09:41	188/ 057	L1T

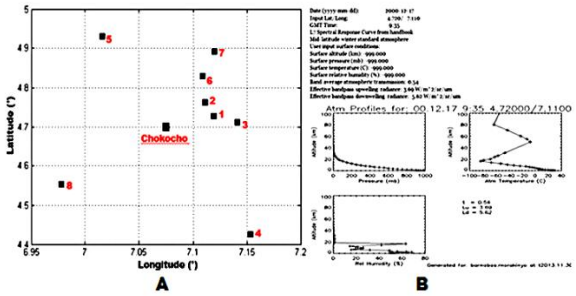

Figure 5: A) Latitude and Longitude of the 9 Flare Sites in Rivers State, Nigeria; B) Atmospheric Correction Parameters and their Profile from the ATMCORR Tool.

Computation of Emissivity (ε) Values

For this research, the four (4) land cover (LC) types (vegetation, soil, built up, and water) with their % identified at these sites during the ground validation period (04/08/2012-21/09/2012) were derived using MATLAB code with cluster analysis. The LC types were clarified using images held within Google Earth and Digital Global (http://browse.digitalglobe.com/imagefinder/public.do), such as WorldView-1 and 2, IKONOS pseudo-true colour images, and Landsat imagery (bands 1-4 and 6), and Red Green Blue (RGB) pseudo-true colour composite images (Morakinyo et al., 2022; Morakinyo, 2024). The method used to estimate the ε value for LC types at these sites is based on the ε values of the 4 LC types present at each site. Each pixel LC type was considered for the entire site, and their ε values (both minimum (min) and maximum (max)) were taken from the literature. Mean of ε value for the LC types for every single pixel obtained from using their (min) and (max) values from the literature was calculated. Average of ε (min) and ε (max) results were obtained for each pixel, and the same procedure was repeated for all pixels in the selected 12-by-12 km area. Table 3 shows the script epsilon values of Land Cover types recorded in the literature (Morakinyo et al., 2021; Morakinyo, 2023).

Science World Journal Vol. 21(No 2) 2026 https://dx.doi.org/10.4314/swj.v21i2.47
www.scienceworldjournal.org
ISSN: 1597-6343 (Online), ISSN: 2756-391X (Print)
Published by Faculty of Science, Kaduna State University

Table 3: Emissivity Values Picked from the Look Up Table (LUT)

Land cover types at the 9 sites investigated	ε Min.	ε Max.	Reference
Short grass Bushes ($\approx$ 100 cm) Densely vegetated areas	0.979 0.960	0.983 0.994 0.980	Labed & Stoll (1991). Labed and Stoll, 1991 Jin and Liang, 2006
Bare soil. Sandy soil Loamy soil		0.960 0.930 0.914	Humes et al., 1994 Hipps, 1989 van de Griend et al., 1991
Water body.	0.950	0.980 0.990	Masuda et al., 1988 Stathopoulou and Cartalis, 2007
Medium built-up area Densely built-up urban		0.964 0.946	Stathopoulou & Cartalis (2007). Stathopoulou and Cartalis, 2007

Therefore, the ε value for each Landsat pixel is a combination of the ε value of the background features, except for any flare present within the pixel. The authors adopted an independent method of using LC types at each site for the correction of ε value rather than Global Land Cover (GLC) data from USGS in order to ensure quality control primarily (Table 3).

Computation of Surface-leaving Radiance

The radiance emitted by a surface at temperature (T) with emissivity (ε_i), in a thermal band i is expressed as $\varepsilon_i B_i(T)$, where $B_i(T)$ is the blackbody radiation described by Planck's law (Schneider & Mauser, 1996). The 'at'-sensor radiance in band i (Li) follows the Radiative Transfer Equation (RTE):

$$L_i(T_i) = \tau_i(\varepsilon_i B_i(T) + (1 - \varepsilon_i)L_i\downarrow + L_i\uparrow \quad (1)$$

Where T_i is defined as the brightness temperature and corresponds to the temperature for which Planck's Law functions equals the 'at'-sensor radiance. The atmospheric correction parameters and $L_i\uparrow$, $L_i\downarrow$, and τ_i, are the atmospheric upwelling radiance, downwelling radiance and transmittance, respectively. ε_i is the emissivity of the land cover types.

The transmittance has a strong inverse dependence on water vapour content, whereas downwelling and upwelling radiances depend on both the atmospheric water vapour and the vertical profiles of air temperature (Coll et al., 2010). Radiance emitted by the surface can be extracted from Equation (1):

$$B_i(T) = ((L_i(T_i) - L_i\uparrow)/\tau_i) - (1 - \varepsilon_i)L_i\downarrow)/\varepsilon_i \quad (2)$$

Retrieval of Land Surface Temperature from Landsat 5 and Landsat 7 Data

The single-channel (SC) methods (Qin et al., 2001; Jimenez-Munoz & Sobrino, 2003; Jimenez-Munoz et al., 2009) that employed the known emissivity and atmospheric parameters used the observations from one TIR channel to retrieve the LST based on the radiative transfer equation (RTE) (Li et al., 2025; Morakinyo, 2026). Single-channel methods are simpler in terms of sensor requirements (Li et al., 2025).

LST, T, can be finally obtained by inverting Planck's function (Eqn. 2) as:

$$T = k_2/Ln(1 + (k_1/B_i(T))) \quad (3)$$

Where k_1 and k_2 are thermal band calibration constants calculated for the Landsat sensor characteristics. For Landsat 5 TM, k_1 = 607.76 ($Wm^{-2}sr^{-1}\mu m^{-1}$) and k_2 = 1260.56 (K); k_1 = 666.09 ($Wm^{-2}sr^{-2}\mu m^{-1}$), and k_2 = 1282.7 K for Landsat 7 ETM+. Coll et al. (2010) showed that using the band-averaged Equation (3) instead of the spectral version yields and overestimation of LST between 0.15 K and 0.3 K depending on the bandwidth, atmospheric humidity and spectral variations of surface emissivity (Richter & Coll, 2002).

Fieldwork/ Ground Validation

The study flaring sites were visited weekly during the period from 04/08/2012 to 21/09/2012 for data quality control and validation of LST results obtained from Landsat 5 and Landsat 7 data. The in situ data obtained are coordinates of the facilities flare stack, relevant features, and points within the site, e.g., open areas, oil-polluted areas, surface temperature (ST), relative humidity, photographs of features and locations, etc. The fieldwork exercises at these sites confirmed that they all have similar LC types (vegetation, some buildings, open land, and water bodies) due to the similar topography of the Niger Delta.

Assessment of Uncertainties Introduced into the Land Surface Temperature Retrieved from Landsat 5 and Landsat 7 Datasets

To determine the uncertainties introduced into LST by applying the calculated atmospheric correction parameters ($L_i\uparrow$, $L_i\downarrow$ and τ_i) obtained for the Landsat 5 and Landsat 7 thermal bands, an uncertainty analysis was undertaken. The difference between the computed mean surface temperature (ST) measured at each flaring site during ground-truthing activities and the combined average LST retrieved from the Landsat 5 and Landsat 7 datasets is used to quantify the error introduced into the LSTs. The methods adopted for the processing of Landsat 5 and Landsat 7 imagery are presented in Figure 6.

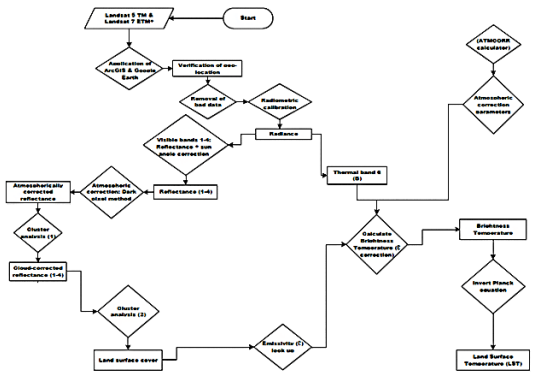

Figure 6: Methodology for the Processing of Landsat 5 and Landsat 7 Data

Science World Journal Vol. 21(No 2) 2026 https://dx.doi.org/10.4314/swj.v21i2.47
www.scienceworldjournal.org
ISSN: 1597-6343 (Online), ISSN: 2756-391X (Print)
Published by Faculty of Science, Kaduna State University

RESULTS

Atmospheric Correction Parameters (Upwelling radiance ($L_i\uparrow$), downwelling radiance ($L_i\downarrow$) and Transmittance (τ)

Some of the values of the computed $L_i\uparrow$, $L_i\downarrow$ and τ obtained for each site investigated are presented in Tables 4-6. The remaining is presented in the appendix. Columns 2 and 3 presented the geographical coordinates of the location of the flare stack within each facility. Columns 4-6 show the computed atmospheric correction parameters obtained from the ATMCORR tool.

Table 4: Atmospheric Correction Parameters from ATMCORR Tool for March 4, 2000

Station	Latitude (θ)	Longitude (λ)	$L\uparrow$ ($Wm^{-2}sr^{-1}\mu m^{-1}$)	$L\downarrow$ ($Wm^{-2}sr^{-1}\mu m^{-1}$)	τ
Elemel	4.728	7.119	3.48	5.31	0.59
Elemell	4.762	7.111	3.43	5.26	0.59
Onne	4.712	7.141	3.50	5.34	0.58
Bonny LNG	4.421	7.163	3.90	5.81	0.54
Rukpokwu	4.930	7.016	3.45	5.28	0.58
Umuroulu	4.829	7.109	3.49	5.35	0.55
Obigbo	4.892	7.120	3.42	5.30	0.55
Elem	4.554	6.978	3.46	5.46	0.57
Chokocho (Centre station)	5.008	7.019	3.29	5.08	0.61

Table 5: Atmospheric Correction Parameters from ATMCORR Tool for December 1, 2000

Station	Latitude (θ)	Longitude (λ)	$L\uparrow$ ($Wm^{-2}sr^{-1}\mu m^{-1}$)	$L\downarrow$ ($Wm^{-2}sr^{-1}\mu m^{-1}$)	τ
Elemel	4.728	7.119	4.54	6.57	0.42
Elemell	4.762	7.111	4.54	6.58	0.42
Onne	4.712	7.141	4.53	6.57	0.42
Bonny LNG	4.421	7.163	4.50	6.54	0.42
Rukpokwu	4.930	7.016	4.53	6.44	0.42
Umuroulu	4.829	7.109	4.55	6.51	0.41
Obigbo	4.892	7.120	4.54	6.53	0.41
Elem	4.554	6.978	4.60	6.56	0.42
Chokocho (Centre station)	5.008	7.019	4.55	6.60	0.42

Table 6: Atmospheric Correction Parameters from ATMCORR Tool for February 6, 2002

Station	Latitude (θ)	Longitude (λ)	$L\uparrow$ ($Wm^{-2}sr^{-1}\mu m^{-1}$)	$L\downarrow$ ($Wm^{-2}sr^{-1}\mu m^{-1}$)	τ
Elemel	4.728	7.119	4.60	6.69	0.43
Elemell	4.762	7.111	4.59	6.68	0.43
Onne	4.712	7.141	4.61	6.69	0.43
Bonny LNG	4.421	7.163	4.72	6.78	0.41
Rukpokwu	4.930	7.016	4.68	6.66	0.42
Umuroulu	4.829	7.109	4.68	6.60	0.43
Obigbo	4.892	7.120	4.70	6.54	0.43
Elem	4.554	6.978	4.72	6.52	0.43
Chokocho (Centre station)	5.008	7.019	4.29	6.32	0.46

Land Surface Temperature

The LSTs retrieved from Landsat 5 and Landsat 7 datasets for the specific site for the period investigated are presented in Tables 7-10. Columns 2-9 presented the LSTs retrieved from the specific scene for the specific year from 2000 to 2013. The LST obtained for each site varies, which could result from variations in the volume and rate of burning gas at the time of the satellite overpass.

The mean LSTs computed for Landsat 5, Landsat 7, and their combined average are shown in Table 11. For Table 11, columns 2 and 3 present the Mean LSTs obtained from Landsat 5 and Landsat 7 datasets, and column 4 shows the combined average of LSTs computed from both of them.

Science World Journal Vol. 21(No 2) 2026 https://dx.doi.org/10.4314/swj.v21i2.47
www.scienceworldjournal.org
ISSN: 1597-6343 (Online), ISSN: 2756-391X (Print)
Published by Faculty of Science, Kaduna State University

Table 7: LST Retrieved from Landsat 5 TM (04/03/2000-18/12/2006)

Flaring site	04/03/2000	1/12/2000	6/2/2002	21/11/2002	12/02/2004	26/11/2004	16/01/2006	18/12/2006
Eleme I	286.046	311.846	309.969	296.280	310.408	320.415	310.512	286.789
Eleme II	284.731	308.493	308.189	306.660	298.837	315.127	312.986	304.867
Onne	282.972	300.262	303.566	308.657	301.132	311.068	308.349	292.016
Bonny LNG	274.491	312.226	313.612	300.126	313.027	311.771	311.085	307.830
Rukpokwu	282.486	305.838	307.126	315.649	309.461	323.702	311.008	307.070
Umurolu	283.471	306.495	313.496	300.599	310.745	314.741	312.473	286.566
Obigbo	285.009	307.563	309.513	314.802	312.817	312.304	308.128	294.094
Elem	278.626	309.086	300.128	307.494	300.417	312.710	308.926	286.981
Chokocho (Centre station)	284.824	310.484	312.708	314.034	302.641	313.307	311.215	300.802

Table 8: LST Retrieved from Landsat 5 TM (06/01/2008-08/03/2013)

Flaring site	06/01/2008	21/11/2008	12/02/2010	13/12/2010	17/01/2012	12/08/2012	03/01/ 2013	08/03/2013
Eleme I	309.220	314.002	308.858	299.768	300.561	300.187	300.003	299.467
Eleme II	306.877	309.367	309.542	309.721	312.307	302.318	302.219	300.635
Onne	304.181	311.610	317.130	306.295	310.866	293.406	315.461	317.882
Bonny LNG	302.149	308.640	311.521	309.765	311.687	310.225	313.425	312.995
Rukpokwu	304.183	300.322	308.627	311.422	315.489	309.036	311.194	314.002
Umurolu	302.106	307.129	323.945	308.718	312.768	311.003	314.521	314.896
Obigbo	301.937	310.461	310.578	324.162	309.687	304.502	315.901	316.421
Elem	304.006	301.418	312.843	310.872	311.416	306.528	313.427	314.967
Chokocho (Centre station)	301.149	312.416	306.270	301.409	308.087	303.812	311.007	313.209

Table 9: LST Retrieved from Landsat 7 ETM+ (04/03/2000-18/12/2006)

Flaring site	04/03/2000	1/12/2000	6/02/2002	21/11/2002	12/02/2004	26/11/2004	16/01/2006	18/12/2006
Eleme I	292.031	308.118	310.997	290.628	293.104	290.320	292.311	290.203
Eleme II	290.438	309.931	309.819	305.666	300.298	306.151	305.130	295.044
Onne	288.713	301.027	304.357	307.865	303.113	312.108	309.835	302.871
Bonny LNG	280.591	314.328	315.361	309.013	314.303	317.177	316.109	312.280
Rukpokwu	288.369	308.583	309.001	314.565	312.095	322.370	315.108	295.884
Umurolu	289.171	307.649	312.350	313.060	314.075	314.791	316.247	300.289
Obigbo	291.011	304.756	310.951	313.482	315.281	316.230	315.081	301.291
Elem	284.751	308.906	301.013	309.749	309.041	313.271	310.089	302.284
Chokocho (Centre station)	290.671	311.048	313.271	312.403	308.264	314.331	312.121	299.067

Table 10: LST Retrieved from Landsat 7 ETM+ (06/01/2008-08/03/2013)

Flaring site	06/01/2008	21/11/2008	12/02/2010	13/12/2010	17/01/2012	12/08/2012	03/01/2013	08/03/ 2013
Eleme I	302.812	292.110	292.891	291.310	289.903	290.231	290.412	289.998
Eleme II	309.875	308.982	306.567	301.030	304.615	302.513	303.213	303.001

Science World Journal Vol. 21(No 2) 2026 https://dx.doi.org/10.4314/swj.v21i2.47
www.scienceworldjournal.org
ISSN: 1597-6343 (Online), ISSN: 2756-391X (Print)
Published by Faculty of Science, Kaduna State University

Onne	302.103	305.437	306.787	304.311	313.211	311.984	309.412	314.626
Bonny LNG	314.468	316.536	311.090	315.430	318.718	317.611	320/448	324.705
Rukpokwu	307.858	309.628	315.457	315.210	321.237	317.511	315.446	317.113
Umurolu	306.765	313.235	314.123	312.408	317.479	316.896	318.743	316.885
Obigbo	305.476	308.110	314.348	316.528	317.623	317.508	311.416	316.200
Elem	307.891	305.101	310.975	311.090	314.327	316.009	315.426	316.990
Chokocho (Centre station)	310.105	312.327	313.240	309.826	314.031	313.212	312.489	312.624

Table 11: Mean LST Retrieved for Landsat 5 and Landsat 7 Data for Each Site

Flaring site	Landsat 5 (Mean LST)	Landsat 7 (Mean LST)	Combined Average LST (K)
Eleme I	304.021	275.954	289.988
Eleme II	305.805	303.890	304.848
Onne	305.303	306.110	305.707
Bonny LNG	307.786	313.656	310.721
Rukpokwu	308.556	311.402	309.979
Umurolu	307.728	311.510	309.619
Obigbo	308.646	310.956	309.801
Elem	304.990	308.557	306.774
Chokocho (Centre station)	306.711	309.939	308.325

Fieldwork/ Ground Validation

The mean weekly surface temperature (ST) results measured at each facility for the period are presented in Table 12. The mean measured surface temperature is presented in column 2; column 3 shows the computed combined average LST. Column 4 shows the difference between the measured ST at each flaring site during the ground-truthing process and the LST retrieved from Landsat datasets.

Table 12: Difference Between the Mean of the ST and LST for Each Facility

Flaring site	Mean ST (K)	Combined Average LST (K)	ST-LST (K)
Eleme I	293.800	289.988	3.812
Eleme II	305.600	304.848	0.752
Onne	318.433	305.707	12.726
Bonny LNG	335.433	310.721	24.712
Rukpokwu	316.900	309.979	06.921
Umurolu	324.667	309.619	14.688
Obigbo	322.433	309.801	12.632
Elem	330.867	306.774	24.093
Chokocho (Centre station)	328.400	308.325	20.075

Uncertainties Introduced into the Retrieved LST by $L_i\uparrow$, $L_i\downarrow$ *and* τ_i

Table 12, column 4, gives the uncertainties introduced into the LSTs obtained from Landsat data by using the atmospheric correction parameters ($L_i\uparrow$, $L_i\downarrow$, and τ_i) computed by the ATMCORR Calculator. Bonny LNG had the highest error, 24.712 K, followed by the Elem oil well at 24.093 K and Chokocho at 20.075 K. These three facilities are located in a typical coastal environment. Bonny LNG is located on the banks of the Atlantic Ocean in the South; the Elem oil well and the Chokocho Flow Station are both in a swampy environment. For Eleme Refinery II, the error introduced into the LSTs is 0.752 K, and for Eleme I, it is 3.812 K. Eleme I has a shared boundary with a small creek. At the same time, Eleme II Refinery is not surrounded by water. Also, the Onne Flow Station with 12.726 K is surrounded by the creek. Generally, the results show that the larger the water body at the site, the higher the error introduced into the LSTs retrieved from the Landsat imagery scene, and vice versa. The results show that the number of water bodies at each site strongly influences Landsat thermal AC parameters obtained from the ATMCORR Tool.

DISCUSSION

Generally, the $L\uparrow$, $L\downarrow$ and τ results obtained (Tables 4-6) in the main text and Tables (A-M) at the appendix varies for all sites. The volumes of water bodies at each site vary, while some facilities are located upland with few or no water bodies. The downwelling and upwelling radiances depend on both the vertical profiles of atmospheric water vapour and air temperature, while transmittance has a strong inverse dependence on the water vapour content (Coll et al., 2010). The LSTs retrieved for all sites also vary, and this could be as a result of the size of the facility (Li et al., 2025); the volume and the rate of the burning gas at the time of satellite

overpass (Morakinyo, 2024; Morakinyo, 2025a); and the number of flare stacks at each facility (Morakinyo et al., 2026; Morakinyo, 2026). In addition, the results for surface temperature (ST) recorded during the ground validation period at each site show that, across all sites, ST is higher than the retrieved LSTs (Table 12). This is supported by Morakinyo et al. (2021), whose paper titled "Methodology and results from ground validation of satellite observations at gas flaring sites in Nigeria" showed that, for all the studied sites, the surface temperatures measured are higher than the LSTs retrieved from the Landsat datasets.

Furthermore, the error introduced into the LSTs retrieved for each site varies due to the computed $L\uparrow$, $L\downarrow$ and τ from the ATMCORR tool used. Bonny LNG and Elem Oil wells produce higher errors, 24.712 K and 24.093 K, respectively, while Eleme II produces the lowest error of 0.752 K. However, the validation of the ATMCORR tool by Barsi et al. (2005) showed a systematic error of $>$ 1.5 K; a bias of 0.5 $\pm$0.8 K; and an error of $\neq$1 K result was recorded by Coll et al. (2010) in their study. The higher error recorded for this study could be as a result of the following; (1) the geographical locations: For example Bonny LNG facility is cited at the coast of the Atlantic Ocean; the Elem oil well is located at the coast of another big river; (2) the difference in the climatic and meteorological conditions between Nigeria and locations used for the validation of the ATMCORR tool e.g. Spain (Coll et al., 2010); and (3) Landsat 5 and Landsat 7 datasets used. For this study, only data from one season (dry) in Nigeria are available due to cloud cover. The unavailability of data from the rainy season is a limitation of this study.

CONCLUSION

Based on the results of the LSTs and the in situ data obtained for this study, it can be concluded that the ATMCORR Calculator can provide an automated method to derive atmospheric correction parameters for the thermal bands of Landsat 5 and Landsat 7 datasets to generate LST in the Niger Delta region of Nigeria.

One of the further studies to be carried out to enhance the analysis is to repeat the use of the ATMCORR Calculator to generate atmospheric correction parameters for Landsat imagery from the Northern region of Nigeria, e.g., the Kaduna Refinery, as a case study. This is because of differences in weather conditions between the Northern and Southern regions of Nigeria.

Stopping gas flaring in Nigeria has not received 100% attention from the Government. Therefore, based on this study, the following recommendations are made. The Nigerian Government should ensure that multinational oil companies operating in the country provide researchers in oil and gas-related fields access to their flaring sites for fieldwork observations and in situ data measurements. In addition, the Nigerian Government should seek a lasting solution to the country's insecurity problem.

Acknowledgements

Thanks to the USGS for providing Landsat data and the MODTRAN ATMCORR Calculator, and to Jill Schwarz for guidance and MATLAB coding.

REFERENCES

Barsi, J. A. (2014). Personal communication: A Solution that Latitude and Longitude with more than one decimal place should not be input into the Calculator: Landsat Project Science Office, Science Systems and Applications, Inc., Greenbelt, United States of America.

Barsi, J. A., Barker, J. L., & Schott, J. R. (2003). An Atmospheric Correction Parameter Calculator for a Single Thermal Band Earth-Sensing Instrument. In Proceedings of the Geoscience and Remote Sensing Symposium 2003 (IGARSS '03), Toulouse, France, 21-25 July 2003.

Barsi, J. A., Schott, J. R., Palluconi, F. D., & Hook, S. J. (2005). Validation of a Web-Based Atmospheric Correction Tool for Single Thermal Band Instruments. In Proceedings of the Earth Observing Systems X, San Diego, CA, USA, 22 August 2005; Volume 5882.

Becker, F., & Li, Z. -L. (1990). Towards a local split-window method over land surfaces. *International Journal of Remote Sensing*, 11, 369–394.

Becker, F., & Li, Z. -L. (1995). Surface temperature and emissivity at various scales: Definition, measurement and related problems. *Remote Sensing of Environment*, 12, 225–253.

Berk, A., Anderson, G. P., Acharya, P. K., & Shettle, E. P. (2011). MODTRAN 5.2.1 User's Manual; Spectral Sciences, Inc.: Burlington, MA, USA.

Campbell, G., Phinn, S. R., Dekker, A. G., & Brando, V. E. (2011). Remote sensing of water quality in an Australian tropical freshwater impoundment using matrix inversion and MERIS images. *Remote Sensing of Environment*, 115, 2402–2414.

Chavez, P. S. (1996). Image-Based Atmospheric Corrections Revisited and Improved. Photogrammetric Engineering and Remote Sensing; Springer: Berlin/Heidelberg, Germany, 62, pp. 1025–1036.

Coll, C., & Caselles, V. (1997). A split-window algorithm for land surface temperature from Advanced Very High Resolution Radiometer data: Validation and algorithm comparison. *Journal of Geophysical Research*, 102, 16697–16713.

Coll, C., Caselles, V., Valor, E., Niclòs, R., Sánchez, J. M., Galve, J. M., & Mira, M. (2007). Temperature and emissivity separation from ASTER data for low-spectral-contrast surfaces. *Remote Sensing of Environment*, 110, 162-175.

Coll, C., Galve, J. M., Sánchez, J. M., & Caselles, V. (2010). Validation of landsat-7 ETM+ thermal-band calibration and atmospheric correction with ground-based measurements. *IEEE Transactions on Geoscience and Remote Sensing*, 48, 547–555.

Coll, C., Caselles, V., Valor, E., & Niclòs, R. (2012). Comparison between different sources of atmospheric profiles for land surface temperature retrieval from single-channel thermal infrared data. *Remote Sensing of Environment*, 117, 199-210.

Coll, C., Garca-Santos, V., Niclòs, R., & Caselles, V. (2016). Test of the MODIS land surface temperature and emissivity separation algorithm with ground measurements over a rice paddy. *IEEE Transactions on Geoscience and Remote Sensing,* 54, 3061-3069.

Duan, S. -B., Li, Z. -L., Wang, C., Zhang, S., Tang, B. -H., Leng, P., & Gao, M. -F. (2018). Land surface temperature retrieval from Landsat 8 single-channel thermal infrared data in combination with NCEP reanalysis data and

ASTER GED product. *International Journal of Remote Sensing*, 40, 1763-1778.

Emberton, S., Chittka, L., Cavallaro, A., & Wang, M. (2015). Sensor Capability and Atmospheric Correction in Ocean Colour Remote Sensing. *Remote Sensing*, 8, 1.

Flood, N., Danaher, T., Gill, T., & Gillingham, S. (2013). An Operational Scheme for Deriving Standardised Surface Reflectance from Landsat TM/ETM+ and SPOT HRG Imagery for Eastern Australia. *Remote Sensing*, 5, 83–109; doi:10.3390/rs5010083

Galve, J. M., Coll, C., Caselles, V., & Valor, E. (2008). An atmospheric radio-sounding database for generating land surface temperature algorithms. *IEEE Transactions of Geoscience and Remote Sensing*, 46, 1547-1557.

Galve, J. M., Sánchez, J. M., Coll, C., & Villodre, J. (2018). A New Single-Band Pixel-by-Pixel Atmospheric Correction Method to Improve the Accuracy in Remote Sensing Estimates of LST: Application to Landsat 7 ETM+. *Remote Sensing*, 10, 826; doi:10.3390/rs10060826

Gillespie, A. R., Matsunaga, T., Rokugawa, S., & Hook, S. J. (1998). Temperature and emissivity separation from Advanced Spaceborne Thermal Emission and Reflection Radiometer (ASTER) images. *IEEE Transactions of Geosciences and Remote Sensing*, 36, 1113–1125.

Google Earth. (2026). Map of Rivers State in the Niger Delta Region, Nigeria; and locations of the Case Study Sites in Rivers State, Nigeria; typical gas flaring at Eleme Petroleum Company Refinery, Bonny LNG Plant, Obigbo Flow Station, Rukpokwu Flow Station and Chokocho Flow Station.

Hu, Y., Liu, L., Liu, L., Peng, D., Jiao, Q., & Zhang, H. (2014). A Landsat-5 Atmospheric Correction Based on MODIS Atmosphere Products and 6S Model. *IEEE Journal of Selected Topics in Applied Earth Observations and Remote Sensing*, 7(5): 1609–1615.

Hulley, G., Hook, S., & Hughes, C. (2014). MODIS MOD21 Land Surface Temperature and Emissivity Algorithm Theoretical Basis Document; Jet Propulsion Laboratory, California Institute of Technology: Pasadena, CA, USA, 12-17 August 2012; (updated: March 2014).

Hipps, L. E. (1989). The Infrared Emissivities of Soil and Artemisia Tridentata and Subsequent Temperature Corrections in a Shrub-steppe Ecosystem. *Remote Sensing of Environment*, 27, 337–342.

Humes, K. S., Kustas, W. P., Moran, M. S., Nichols, W. D., & Weltz, M. A. (1994). Variability of Emissivity and Surface Temperature Over a Sparsely Vegetated Surface. *Water Resources Research*, 30(5), 1299–1310.

Inamdar, A. K., French, A., Hook, S., Vanghan, G., & Luckett, W. (2008). Land surface temperature retrieval at high spatial and temporal resolutions over the south-western United States. *Journal of Geophysical Research: Atmospheres,* 113(D7), 1–18.

Jiménez-Muñoz, J. C., & Sobrino, J. A. (2003). A Generalized Single-Channel Method for

Retrieving Land Surface Temperature from Remote Sensing Data. *Journal of Geophysical Research*, 108, doi:10.1029/2003JD003480.

Jiménez-Muñoz, J. C., Cristóbal, J., Sobrino, J. A., Soria, G., Ninyerola, M., & Pons, X. (2009). Revision of the Single-Channel Algorithm for Land Surface Temperature Retrieval From Landsat Thermal-Infrared Data. *IEEE Transactions on Geoscience and Remote Sensing*, 47(1): 339–349.

Jin, M., & Liang, S. (2006). An Improved Land Surface Emissivity Parameter for Land Surface Models Using Global Remote Sensing Observations. *Journal of Climate*, 19, 2867–2881.

Kokhanovsky, A. A., & de Leeuw, G. (2009). Satellite Aerosol Remote Sensing over Land. 1st Edition, Springer: Berlin/Heidelberg, Germany, p. 388.

Kondratyev, K. Y., Kozoderov, V. V., & Smokty, O. I. (1992). Remote Sensing of the Earth from Space: Atmospheric Correction; Springer: Berlin/Heidelberg, Germany.

Labed, J., & Stoll, M. P. (1991). Spatial Variability of Land Surface Emissivity in the Thermal Infrared Band: Spectral Signature and Effective Surface Temperature. *Remote Sensing of Environment*, 38, 1–7.

Li, H., Liu, Q., Du, Y., Jiang, J., & Wang, H. (2013). Evaluation of the NCEP and MODIS atmospheric products for single-channel land surface temperature retrieval with ground measurements: A case study of HJ-1B IRS data. *IEEE Journal of Selected Topics in Applied Earth Observation and Remote Sensing*, 6, 1399–1408.

Li, X., Wu, H., Li, Z., Sobrino, J., Zhang, X., & Cheng, Y. (2025). A novel correlation-hypothesis-based single-channel method for land surface temperature retrieval with reduced atmospheric dependency. *Remote Sensing of Environment*, 327, 114817

Liou, K. N. (2002). An Introduction to Atmospheric Radiation. 2nd Edition, Academic Press: San Diego, CA, USA, p. 583.

Liu, G., Li, Y. M., Lyu, H., Wang, S., Du, C. G., & Huang, C. C. (2016). An improved land target-based atmospheric correction method for Lake Taihu. *IEEE Journal of Selected Topics in Applied Earth Observation and Remote Sensing*, 9, 793–803.

Madeira, C. (2002). Generalized split-window algorithm for retrieving land surface temperature from MSG/SEVIRI data. In Proceedings of the Land Surface Analysis SAF Training Workshop, Lisbon, Portugal, July 8-10, pp. 42–47.

Markham, B. L., & Barker, J. L. (1985). Spectral Characterization of the Landsat Thematic Mapper Sensors. *International Journal of Remote Sensing*, 6, 697–716. https://doi.org/10.1080/01431168508948492

Masek, J., Vermote, E., Saleous, N., Wolfe, R., Hall, F., Huemmrich, K., Gao, F., Kutler, J., & Lim, T. K. (2006). A Landsat surface reflectance dataset for North America, 1990-2000. *IEEE Geoscience and Remote Sensing Letters*, 3, 68–72.

Masuda, K., Takashima, T., & Takayama, Y. (1988). Emissivity of Pure and Sea Waters for the Model Sea Surface in the Infrared Window Regions. *Remote Sensing of Environment,* 24, 313–329.

Mather, P. M. (2004). Computer processing of remotely sensed images: An Introduction, 3rd

Edition. West Sussex, England, John Wiley and Sons.

McCarthy, S. C., Gould, R. W., Richman, J., Kearney, C., & Lawson, A. (2012). Impact of Aerosol Model Selection on Water-Leaving Radiance Retrievals from Satellite

Ocean Colour Imagery. *Remote Sensing*, 4, 3638–3665.

McCarville, D., Buenemann, M., Bleiweiss, M., & Barsi, J. A. (2011). Atmospheric Correction of Landsat Thermal Infrared Data: A Calculator Based on North America Regional Reanalysis (NARR). ASPRS Annual Conference, Milwaukee, Wisconsin: 12.

Meng, X., & Cheng, J. (2018). Evaluating Eight Global Reanalysis Products for Atmospheric Correction of Thermal Infrared Sensor: Application to Landsat 8 TIRS10 Data. *Remote Sensing,* 10, 474.

Morakinyo, B. O. (2015). Flaring and Pollution Detection in the Niger Delta Using Remote Sensing. PhD Thesis, School of Marine Science and Engineering, University of Plymouth, Plymouth, United Kingdom.

Morakinyo, B. O., Lavender, S., & Abbott, V. (2021). The Methodology and Results from Ground Validation of Satellite Observations at Gas Flaring Sites in Nigeria. *International Journal of Environment and Geoinformatics (IJEGEO)*, 8(3), 290–300, Doi. 10.30897/ijegeo.749664

Morakinyo, B. O., Lavender, S., & Abbott, V. (2022). Investigation of Potential Prevailing Wind Impact on Land Surface Temperature at Gas Flaring Sites in the Niger Delta, Nigeria. *International Journal of Environment and Geoinformatics (IJEGEO)*, 9(1), 179–190.

Morakinyo, B. O. (2023). Detection of Impacts of Gas Flaring in the Environment: Application of Landsat Earth Observation Data. *BAZE University Journal of Entrepreneurship and Interdisciplinary Studies (BUJEIS),* 2(1): 74–89.

Morakinyo, B. O. (2024). Time Series Analysis of Earth Observation Satellites Data for Evaluating Changes in Vegetation Cover and Health at Flaring Sites. *Academic Platform Journal of Natural Hazards and Disaster Management (APJHAD)*. Faculty of Engineering, Sakarya University, Turkey, 5(2), 76–100, DOI: 10.52114/apjhad. 1557231

Morakinyo, B. O. (2025a). Remote Sensing of Spatial and Temporal Mapping of Flare Impacts in the Niger Delta, Nigeria. *Journal of International Environmental Application and Science (JIEAS)*. Faculty of Engineering and Natural Sciences, Konya Technical University, Turkey, 20, 98–115.

Morakinyo, B. O., Lavender, S., & Abbott, V. (2025b). Detection of Potentially Gas Flaring-related Pollution on Vegetation Cover and Its Health Using Remotely Sensed Data in the Niger Delta. *Nile Journal of Engineering and Applied Science (NJEAS)*. Nile University of Nigeria, Abuja, 3(1), 49-58, DOI: https://doi.org/10.5455/NJEAS.287918

Morakinyo, B. O., & Akubue, J. A. (2026). Surveying and Geoinformatics Profession and Construction Industry: A Case Study of BAZE University Teaching Hospital (BUTH), Abuja, Nigeria. *FUDMA Journal of Sciences (FJS)*, Faculty of Science, Federal University Dutsin-Ma, 10(1), 124–140, DOI: https://doi.org/10.33003/fjs-2025-1001-4515

Morakinyo, B. O. (2026). Retrieval of Land Surface Temperature from Earth Observation Satellites for Gas Flaring Sites in the Niger Delta, Nigeria. *FUDMA Journal of Sciences (FJS)*, Faculty of Science, Federal University Dutsin-Ma, 10(3), 173–187, DOI: https://doi.org/10.33003/fjs-2026-1003-4772

Niclòs, R., Galve, J. M., Valiente, J. A., Estrela, M. J., & Coll, C. (2011). Accuracy assessment of land surface temperature retrievals from MSG2-SEVIRI data. *Remote Sensing of Environment*, 115, 2126-2140.

Niclòs, R., Pérez-Planells, L., Coll, C., Valiente, J. A., & Valor, E. (2018). Evaluation of the S-NPP VIIRS land surface temperature product using ground data acquired by an autonomous system at a rice paddy. *ISPRS Journal of Photogrammetry and Remote Sensing*, 135, 1-12.

Otukei, J. R., & Blaschke, T. (2011). You Know The Temperature at a weather station, but do you know it anywhere else? Assessing the Land Surface Temperature Using Landsat ETMplus Data. Proceedings of the First Conference on Advances in Geomatics Research: 169–179.

Padró, J. C., Pons, X., Aragonés, D., Díaz-Delgado, R., García, D., Bustamante, J., Pesquer, L., Domingo-Marimon, C., González-Guerrero, O., Cristóbal, J., Doktor, D., & Lange, M. (2017). Radiometric Correction of Simultaneously Acquired Landsat-7/Landsat-8 and Sentinel-2A Imagery Using Pseudo-invariant Areas (PIA): Contributing to the Landsat Time Series Legacy. *Remote Sensing*, 9, 1319; doi:10.3390/rs9121319

Prata, A. J. (2002). Land Surface Temperature Measurement from Space: AATSR Algorithm Theoretical Basis Document; Technical Report, 34; CSIRO Atmospheric Research: Aspendale, Australia.

Price, J. C. (1984). Land surface temperature measurements from the split-window channels of the NOAA 7 AVHRR. *Journal of Geophysical Research*, 89, 7231-7237.

Qin, Z., Olmo, G. D., & Karnieli, A. (2001). Derivation of Split Window Algorithm and Its Sensitivity Analysis For Retrieving Land Surface Temperature From NOAA-Advanced Very High Resolution Radiometer Data. *Geophysical Research,* 22655–22670.

Qin, Q., Zhang, N., Nan, P., & Chai, L. (2011). Geothermal Area Detection Using Landsat ETMplus Thermal Infrared Data and Its Mechanistic Analysis: A Case Study in Tengchong, China. *International Journal of Applied Earth Observation and Geoinformation,* 13, 552-559.

Richter, R., & Coll, C. (2002). Band-pass resampling effects for the retrieval of surface emissivity. *Applied Optics*, 41, 3523–3529.

Schneider, K., & Mauser, W. (1996). Processing and accuracy of Landsat TM data for lake surface temperature measurement. *International Journal of Remote Sensing*, 17(11), 2027-2041.

Schott, J. R. (1989). Image Processing of Thermal Infrared Images. *Photogrammetric Engineering and Remote Sensing*, 55: 1311–1321.

Schroeder, T. A., Cohen, W. B., Song, C., Canty, M. J., & Yang, Z. (2006). Radiometric correction of multi-temporal Landsat data for characterization of early successional forest patterns in western Oregon. *Remote Sensing of Environment*, 103, 16–26.

Stathopoulou, M., & Cartalis, C. (2007). Daytime Urban Heat Island from Landsat ETMplus and Corine Land Cover Data: An Application to Major Cities in Greece. *Solar Energy*, 81, 358–368.

Trigo, I. T., Monteiro, F., Olesen, E., & Kabsch, E. (2008). An assessment of remotely sensed land surface temperature. *Journal of Geophysical Research*, 113, D17108.

Turner, R. E., Malila, W. A., & Nalepha, R. F. (1971). Importance of atmospheric scattering in remote sensing. In Proceedings of the Seventh International Symposium on Remote Sensing of Environment, Ann Arbor, MI, USA, 17-21 May, 3, pp. 1651–1697.

USGS. (2015). Landsat 7 (L7) Enhanced Thematic Mapper Plus (ETM+) Level 1 (L1) Data Format Control Book (DFCB). U.S. Geological Survey (USGS) Earth Resources Observation and Science (EROS) Center, 47914 252nd Street, Sioux Falls, SD 57198.

van de Griend, A. A., Owe, M., Groen, M., & Stoll, M. P. (1991). Measurement and Spatial Variation of Thermal Infrared Surface Emissivity in a Savannah Environment. *Water Resources Research,* 27, 371–379.

Vicente-Serrano, S. M., Perez-Cabello, F., & Lasanta, T. (2008). Assessment of radiometric correction techniques in analyzing vegetation variability and change using time series of Landsat images. *Remote Sensing of Environment*, 112, 3916–3934.

Wan, Z., & Dozier, J. (1996). A Generalized Split-Window Algorithm for Retrieving Land Surface Temperature Measurement from Space. *IEEE Transactions on Geoscience and Remote Sensing,* 34, 892–905.

Wan, Z. (1999). MODIS Land Surface Temperature. Algorithm Theoretical Basis Document; NAS5-31370; University of California: Santa Barbara, CA, USA.

Wan, Z. (2008). New refinements and validation of the MODIS Land-Surface Temperature/Emissivity products. *Remote Sensing of Environment*, 112, 59–74.

Yu, Y., Privette, J. L., & Pinheiro, A. (2005). Analysis of the NPOESS VIIRS land surface temperature algorithm using MODIS data. *IEEE Transactions of Geosciences and Remote Sensing*, 43, 2340–2350.

Zhu, W., Tian, Y. Q., Yu, Q., & Becker, B. L. (2013). Using Hyperion imagery to monitor the spatial and temporal distribution of coloured dissolved organic matter in estuarine and coastal regions. *Remote Sensing of Environment*, 134, 342–354.

Zhu, W., & Xia, W. (2023). Effects of Atmospheric Correction on Remote Sensing Statistical Inference in an Aquatic Environment. *Remote Sensing*, 15, 1907, https://doi.org/10.3390/rs15071907

APPENDIX

The remaining values of the computed $L\uparrow,\downarrow$ and τ obtained for each site investigated are presented in Tables A-M

Table A: Atmospheric Correction Parameters from ATMCORR Tool for November 21, 2002

Station	Latitude (θ)	Longitude (λ)	$L\uparrow$ ($Wm^{-2}sr^{-1}\mu m^{-1}$)	$L\downarrow$ ($Wm^{-2}sr^{-1}\mu m^{-1}$)	τ
Elemel	4.728	7.119	4.77	6.79	0.40
Elemell	4.762	7.111	4.77	6.79	0.40
Onne	4.712	7.141	4.77	6.79	0.40
Bonny LNG	4.421	7.163	4.79	6.82	0.39
Rukpokwu	4.930	7.016	4.76	6.80	0.40
Umuroluu	4.829	7.109	4.76	6.79	0.38
Obigbo	4.892	7.120	4.75	6.81	0.39
Elem	4.554	6.978	4.77	6.80	0.40
Chokocho (Centre station)	5.008	7.019	4.64	6.70	0.42

Table B: Atmospheric Correction Parameters from ATMCORR Tool for February 12, 2004

Station	Latitude (θ)	Longitude (λ)	$L\uparrow$ ($Wm^{-2}sr^{-1}\mu m^{-1}$)	$L\downarrow$ ($Wm^{-2}sr^{-1}\mu m^{-1}$)	τ
Elemel	4.728	7.119	4.68	6.73	0.42
Elemell	4.762	7.111	4.68	6.73	0.42
Onne	4.712	7.141	4.69	6.74	0.41
Bonny LNG	4.421	7.163	4.78	6.82	0.40
Rukpokwu	4.930	7.016	4.73	6.80	0.42
Umuroluu	4.829	7.109	4.70	6.81	0.41
Obigbo	4.892	7.120	4.68	6.78	0.41
Elem	4.554	6.978	4.72	6.76	0.42
Chokocho (Centre station)	5.008	7.019	4.87	6.91	0.35

Table C: Atmospheric Correction Parameters from ATMCORR Tool for November 26, 2004

Station	Latitude (θ)	Longitude (λ)	$L\uparrow$ ($Wm^{-2}sr^{-1}\mu m^{-1}$)	$L\downarrow$ ($Wm^{-2}sr^{-1}\mu m^{-1}$)	τ
Elemel	4.728	7.119	5.09	7.18	0.33
Elemell	4.762	7.111	5.09	7.18	0.33
Onne	4.712	7.141	5.09	7.18	0.33
Bonny LNG	4.421	7.163	5.07	7.14	0.34
Rukpo	4.93	7.016	5.08	7.16	0.

kwu	0				33
Umurolu	4.829	7.109	5.07	7.16	0.33
Obigbo	4.892	7.120	5.07	7.14	0.34
Elem	4.554	6.978	5.09	7.18	0.33
Chokocho (Centre station)	5.008	7.019	5.06	7.14	0.35

Table D: Atmospheric Correction Parameters from ATMCORR Tool for January 16, 2006

Station	Latitude (θ)	Longitude (λ)	$L\uparrow$ ($Wm^{-2}sr^{-1}\mu m^{-1}$)	$L\downarrow$ ($Wm^{-2}sr^{-1}\mu m^{-1}$)	τ
Elemel	4.728	7.119	4.44	6.52	0.43
Elemell	4.762	7.111	4.44	6.51	0.43
Onne	4.712	7.141	4.45	6.52	0.43
Bonny LNG	4.421	7.163	4.56	6.63	0.42
Rukpokwu	4.930	7.016	4.50	6.50	0.42
Umurolu	4.829	7.109	4.46	6.51	0.43
Obigbo	4.892	7.120	4.48	6.58	0.43
Elem	4.554	6.978	4.45	6.57	0.42
Chokocho (Centre station)	5.008	7.019	4.09	6.06	0.47

Table E: Atmospheric Correction Parameters from ATMCORR Tool for December 18, 2006

Station	Latitude (θ)	Longitude (λ)	$L\uparrow$ ($Wm^{-2}sr^{-1}\mu m^{-1}$)	$L\downarrow$ ($Wm^{-2}sr^{-1}\mu m^{-1}$)	τ
Elemel	4.728	7.119	3.88	5.80	0.52
Elemell	4.762	7.111	3.85	5.76	0.53
Onne	4.712	7.141	3.90	5.83	0.52
Bonny LNG	4.421	7.163	4.18	6.14	0.48
Rukpokwu	4.930	7.016	4.00	6.00	0.50
Umurolu	4.829	7.109	4.10	5.97	0.51
Obigbo	4.89	7.120	3.90	5.98	0.
	2				52
Elem	4.554	6.978	4.01	6.00	0.51
Chokocho (Centre station)	5.008	7.019	3.71	5.60	0.55

Table F Atmospheric Correction Parameters from ATMCORR Tool for January 6, 2008

Station	Latitude (θ)	Longitude (λ)	$L\uparrow$ ($Wm^{-2}sr^{-1}\mu m^{-1}$)	$L\downarrow$ ($Wm^{-2}sr^{-1}\mu m^{-1}$)	τ
Elemel	4.728	7.119	4.96	7.11	0.34
Elemell	4.762	7.111	4.96	7.11	0.34
Onne	4.712	7.141	4.95	7.11	0.34
Bonny LNG	4.421	7.163	4.93	7.06	0.35
Rukpokwu	4.930	7.016	4.94	7.09	0.35
Umurolu	4.829	7.109	4.96	7.10	0.34
Obigbo	4.892	7.120	4.95	7.10	0.34
Elem	4.554	6.978	4.95	7.11	0.35
Chokocho (Centre station)	5.008	7.019	4.96	7.12	0.34

Table G: Atmospheric Correction Parameters from ATMCORR Tool for November 21, 2008

Station	Latitude (θ)	Longitude (λ)	$L\uparrow$ ($Wm^{-2}sr^{-1}\mu m^{-1}$)	$L\downarrow$ ($Wm^{-2}sr^{-1}\mu m^{-1}$)	τ
Elemel	4.728	7.119	4.93	6.94	0.38
Elemell	4.762	7.111	4.92	6.93	0.39
Onne	4.712	7.141	4.93	6.95	0.38
Bonny LNG	4.421	7.163	4.99	6.98	0.37
Rukpokwu	4.930	7.016	4.96	6.96	0.38
Umurolu	4.829	7.109	4.98	6.96	0.38
Obigbo	4.892	7.120	4.96	6.94	0.37
Elem	4.554	6.978	4.94	6.95	0.38
Choko	5.00	7.019	4.90	6.93	0.

Science World Journal Vol. 21(No 2) 2026 https://dx.doi.org/10.4314/swj.v21i2.47
www.scienceworldjournal.org
ISSN: 1597-6343 (Online), ISSN: 2756-391X (Print)
Published by Faculty of Science, Kaduna State University

cho (Centre station)	8				39

Table H: Atmospheric Correction Parameters from ATMCORR Tool for February 12, 2010

Station	Latitude (θ)	Longitude (λ)	$L\uparrow$ ($Wm^{-2}sr^{-1}\mu m^{-1}$)	$L\downarrow$ ($Wm^{-2}sr^{-1}\mu m^{-1}$)	τ
Elemel	4.728	7.119	5.34	7.42	0.32
Elemell	4.762	7.111	5.34	7.43	0.32
Onne	4.712	7.141	5.33	7.42	0.32
Bonny LNG	4.421	7.163	5.30	7.36	0.33
Rukpokwu	4.930	7.016	5.32	7.40	0.32
Umurolu	4.829	7.109	5.34	7.42	0.33
Obigbo	4.892	7.120	5.34	7.40	0.32
Elem	4.554	6.978	5.33	7.31	0.32
Chokocho (Centre station)	5.008	7.019	5.06	7.14	0.35

Table I: Atmospheric Correction Parameters from ATMCORR Tool for December 13, 2010

Station	Latitude (θ)	Longitude (λ)	$L\uparrow$ ($Wm^{-2}sr^{-1}\mu m^{-1}$)	$L\downarrow$ ($Wm^{-2}sr^{-1}\mu m^{-1}$)	τ
Elemel	4.728	7.119	4.01	5.99	0.50
Elemell	4.762	7.111	3.98	5.95	0.50
Onne	4.712	7.141	4.03	6.02	0.50
Bonny LNG	4.421	7.163	4.27	6.29	0.46
Rukpokwu	4.930	7.016	4.00	6.14	0.49
Umurolu	4.829	7.109	4.02	6.09	0.53
Obigbo	4.892	7.120	3.99	6.01	0.55
Elem	4.554	6.978	4.01	5.53	0.56
Chokocho (Centre station)	5.008	7.019	3.28	5.07	0.58

Table J: Atmospheric Correction Parameters from ATMCORR Tool for January 17, 2012

Station	Latitude (θ)	Longitude (λ)	$L\uparrow$ ($Wm^{-2}sr^{-1}\mu m^{-1}$)	$L\downarrow$ ($Wm^{-2}sr^{-1}\mu m^{-1}$)	τ
Elemel	4.728	7.119	3.16	4.92	0.62
Elemell	4.762	7.111	3.14	4.90	0.62
Onne	4.712	7.141	3.17	4.94	0.62
Bonny LNG	4.421	7.163	3.31	5.08	0.60
Rukpokwu	4.930	7.016	3.22	5.02	0.64
Umurolu	4.829	7.109	3.20	5.00	0.64
Obigbo	4.892	7.120	3.22	4.89	0.68
Elem	4.554	6.978	3.21	4.65	0.69
Chokocho (Centre station)	5.008	7.019	2.36	3.76	0.70

Table K: Atmospheric Correction Parameters from ATMCORR Tool for August 12, 2012

Station	Latitude (θ)	Longitude (λ)	$L\uparrow$ ($Wm^{-2}sr^{-1}\mu m^{-1}$)	$L\downarrow$ ($Wm^{-2}sr^{-1}\mu m^{-1}$)	τ
Eleme l	4.728	7.119	4.25	6.24	0.45
Eleme ll	4.762	7.111	4.25	6.25	0.45
Onne	4.712	7.141	4.24	6.23	0.45
Bonny LNG	4.421	7.163	4.17	6.07	0.45
Rukpokwu	4.930	7.016	4.20	6.24	0.45
Umurolu	4.829	7.109	4.24	6.22	0.45

Science World Journal Vol. 21(No 2) 2026 https://dx.doi.org/10.4314/swj.v21i2.47
www.scienceworldjournal.org
ISSN: 1597-6343 (Online), ISSN: 2756-391X (Print)
Published by Faculty of Science, Kaduna State University

Obigbo	4.892	7.120	4.24	6.28	0.45
Elem	4.554	6.978	4.26	6.28	0.45
Chokocho (Centre station)	5.008	7.019	4.28	6.31	0.45

Table L: Atmospheric Correction Parameters from ATMCORR Tool for January 03, 2013

Station	Latitude (θ)	Longitude (λ)	$L\uparrow$ ($Wm^{-2}sr^{-1}\mu m^{-1}$)	$L\downarrow$ ($Wm^{-2}sr^{-1}\mu m^{-1}$)	τ
Eleme I	4.728	7.119	4.02	6.24	0.44
Eleme II	4.762	7.111	4.13	6.24	0.45
Onne	4.712	7.141	4.24	6.25	0.45
Bonny LNG	4.421	7.163	4.18	6.08	0.43
Rukpokwu	4.930	7.016	4.18	6.25	0.45
Umurolu	4.829	7.109	4.25	6.23	0.44
Obigbo	4.892	7.120	4.26	6.27	0.43
Elem	4.554	6.978	4.25	6.28	0.44
Chokocho (Centre station)	5.008	7.019	4.27	6.32	0.45

Table M: Atmospheric Correction Parameters from ATMCORR Tool for March 08, 2013

Station	Latitude (θ)	Longitude (λ)	$L\uparrow$ ($Wm^{-2}sr^{-1}\mu m^{-1}$)	$L\downarrow$ ($Wm^{-2}sr^{-1}\mu m^{-1}$)	τ
Eleme I	4.728	7.119	4.24	6.23	0.41
Eleme II	4.762	7.111	4.25	6.24	0.45
Onne	4.712	7.141	4.23	6.23	0.45
Bonny LNG	4.421	7.163	4.19	6.26	0.43
Rukpokwu	4.930	7.016	4.21	6.24	0.45
Umurolu	4.829	7.109	4.23	6.23	0.44
Obigbo	4.892	7.120	4.23	6.27	0.45
Elem	4.554	6.978	4.25	6.28	0.44
Chokocho (Centre station)	5.008	7.019	4.27	6.30	0.45